Numerical Analysis of the Propagation Characteristics of Multiangle Multislot Coaxial Cable Using Moment Method

Seon-Taek Kim, Gi-Ho Yun, and Han-Kyu Park, *Senior Member, IEEE*

***Abstract*— In this paper, multiangle multislot coaxial cable is analyzed qualitatively and quantitatively. This is the extended result of the previous studies for single-slot coaxial cable. The properties of single-slot coaxial cable have been studied by many authors, especially for the surface-wave type. However, slotted coaxial cable utilizing leaky wave has not been treated rigorously despite its wide use. In this paper, a numerical analysis of leaky coaxial cable with multiangle multislot configuration is performed to obtain many useful results, which is impossible employing the approximate model frequently used in this area. Using the moment method, the propagation constant has been obtained for the leaky coaxial cable as a function of various parameters. Several slot configurations are considered to give insight into the properties of coupling loss and transmission loss complicated by simultaneous existence of leaky and surface wave.**

***Index Terms*— Coaxial aperture anten- nas, leaky-wave antennas, moment methods, periodic structures, surface waves, traveling-wave antennas.**

I. Introduction

SLOTTED coaxial cables are frequently used in many communication areas such as buildings, mines, tunnels, subways, etc. where propagation from a conventional discrete antenna is impossible. Currently available slotted coaxial cables fall into two groups. One is surface-wave type, and the other is leaky-wave type. The former is usually called a radiative coaxial cable (RCX), and the latter a leaky coaxial cable (LCX).

RCX has several types available. Some have loosely woven outer braids, and others have periodically holed outer conductors. A third type has a uniform axial slot in the outer conductor. LCX has evolved from simple 2- to 14-slot configuration. The most significant difference between the periodically slotted RCX and LCX is their pitch, the length between adjacent slot-groups. The pitch of LCX is much longer than that of RCX. As a result, the radiation and coupling of RCX come from surface wave, whereas the coupling of LCX is due to leaky wave.

The propagation characteristics of RCX have been studied by many authors. It is well known that RCX has two independently propagating modes: bifilar and monofilar mode. The bifilar mode carries most of its energy inside the cable with small energy outside, and *vice versa* for the monofilar mode. The pair of the propagation modes and the concept of surface transfer impedance were used in determining the performance of braided coaxial cable in a complicated environment [1]–[3]. General analyses were performed for simple geometry of braided coaxial cable in free space [4], [5]. The uniform axially slotted RCX was analyzed by variational method in [6]–[9]. The periodically holed RCX was also analyzed in [10]–[12].

LCX analyses have been focused on the extension of available frequency bands. To this end, many papers utilized the sinusoidal distribution of slot angles [13]–[15]. Recently super broad-band LCX has been reported using this principle [16]. To the authors' knowledge, however, a rigorous analysis of LCX other than approximations has not been attempted so far. In this paper, a general problem of multiangle multislot LCX is considered for the first time. To solve the problem, field distributions are assumed inside and outside LCX, and moment method is applied using boundary conditions. As a result, propagation constant and field distributions are obtained so that the coupling and transmission loss can be calculated.

II. Basic Principle of Frequency Bandwidth Expansion

The principle of frequency bandwidth expansion is easily explained by approximating LCX as an infinite line with periodic magnetic current distribution using the equivalence principle. The mth (m: integer) harmonic component of the periodic source expressed in Fourier series generates the mth spatial harmonic in free space [17]. Usually only the negative harmonic components $(m \leq -1)$ can produce leaky waves in the following frequency ranges:

$$-\frac{c}{1+\sqrt{\epsilon_r}}\frac{m}{p} < f < -\frac{c}{\sqrt{\epsilon_r}-1}\frac{m}{p}, \qquad m = -1, -2, -3, \cdots \quad (1)$$

where

- c velocity of the light;
- ϵ_r relative permittivity of the dielectric material between the coaxial conductors;
- p period of the magnetic current distribution.

Actually the upper frequency limit of (1) takes value beyond the operational frequency bands. Therefore, for the frequency ranges considered, (1) can be rewritten in a normalized form after dividing the lower frequency limit by $c/(1+\sqrt{\epsilon_r})$:

$$f_N > -\frac{m}{p}, \qquad m = -1, -2, -3, \cdots . \quad (2)$$

Manuscript received October 29, 1996; revised December 10, 1997.

S.-T. Kim is with the Information and Telecommunications R&D Center, Hyundai Electronics Industries Co., Ltd., Korea.

G.-H. Yun and H.-K. Park are with the Radio Communications Research Center, Yonsei University, Seoul, 120-749 Korea.

Publisher Item Identifier S 0018-9480(98)02026-2.

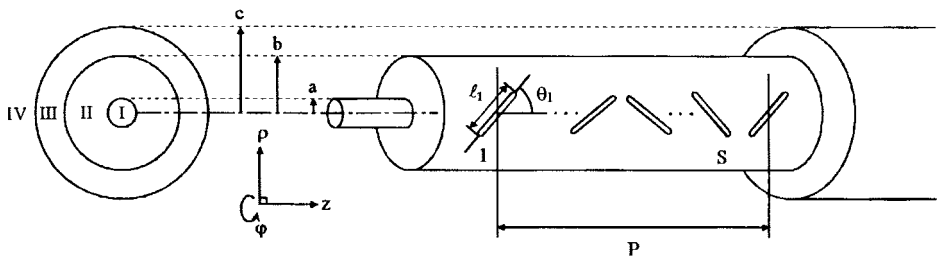

Fig. 1. Geometry of problem.

Hence, the mth spatial harmonic $(m \leq -1)$ produces leaky wave above the normalized frequency of $-m/p$.

Since leaky waves with different beam directions interfere with each other and cause fluctuation in the radiated fields, it is required to suppress the higher order spatial harmonics except for $m = -1$. To this end, the current distribution of the line source is made to be sinusoidal having p as period, which is then transformed into the slot arrangement in the original geometry by letting the angle distribution of slots be sinusoidal. This is possible only in discrete manner because of the finite number of slots per period (or pitch). From the sampling theory, the higher the sampling rate is, which corresponds to the increase of the number of slots per pitch, the wider the available band. For example, two-slot LCX with two slots per pitch has available normalized frequency bands from $1/p$ to $3/p$ where only $m = -1$ spatial harmonic radiates as leaky wave. Six-slot LCX with six slots per pitch has wider bandwidth from $1/p$ to $7/p$.

III. Formulation of Problem

Although the theory in Section II explains the behavior of LCX well, it is only by approximations. For physical geometry of LCX the higher order spatial harmonics radiate even in the single mode zone. Therefore, it is a practical problem that the real field distributions of LCX are very sensitive to the slot arrangements. Moreover, qualitatively useful values of coupling loss and transmission loss cannot be obtained from the previous theory.

A newly developed analysis in this section can be useful at this point since the analysis deals with the physical geometry of LCX so that the propagation constant and the field distributions can be determined.

A. Geometry of the Problem

The geometry of the problem is shown in Fig. 1. LCX has infinite length in free space with the inner conductor of radius a and the outer conductor of radius b. The outer conductor is assumed to have perfect conductivity and negligible thickness. It is coated with dielectric sheath with radius c. Source is assumed to be at $z = \pm\infty$, so the problem is a source-free case. Pitch, the slot-group spacing, is p. S is the number of slots per pitch, and the sth $(s = 1, 2, \cdots, S)$ slot has length l_s and angle θ_s.

B. Field Representation

For each region in Fig. 1, it is convenient to define electric and magnetic Hertz vectors Π_e and Π_m, respectively, that have only z-components in terms of cylindrical coordinate system (ρ, ϕ, z). These Hertz vectors must satisfy Floquet's theorem to include the effect of the periodic slot arrangements.

Therefore,

$$\Pi_e^{(i)} = \sum_{m=-\infty}^{\infty}\sum_{n=-\infty}^{\infty} [A_{mn}^{(i)} I_n(\beta_m^{(i)}\rho) + B_{mn}^{(i)} K_n(\beta_m^{(i)}\rho)] \cdot e^{jn\phi} e^{-j\alpha_m z}$$
$$\Pi_m^{(i)} = \sum_{m=-\infty}^{\infty}\sum_{n=-\infty}^{\infty} [C_{mn}^{(i)} I_n(\beta_m^{(i)}\rho) + D_{mn}^{(i)} K_n(\beta_m^{(i)}\rho)] \cdot e^{jn\phi} e^{-j\alpha_m z}, \qquad i = \mathrm{I}, \mathrm{II}, \mathrm{III}, \mathrm{IV} \tag{3}$$

where

$$\alpha_m = \alpha_o + \frac{2\pi}{p} m = \alpha_o' + \frac{2\pi}{p} m + j\alpha_o''$$
$$\beta_m^{(i)} = \sqrt{\alpha_m^2 - k_i^2}$$
$$k_i = \varpi\sqrt{\mu_o \epsilon_i} \quad \epsilon_i = \epsilon_i' - j\epsilon_i''$$
$$\epsilon_i'' = \begin{cases} \sigma/\varpi, & i = \mathrm{I} \\ \epsilon_i' \tan\delta_{\mathbf{i}}, & i = \mathrm{II}, \mathrm{III} \end{cases}$$

α_m is the axial propagation constant of the mth spatial harmonic. $\beta_m^{(i)}$ is the radial propagation constant that determines whether the mth spatial harmonic is a leaky or surface wave in region i. k_i and ϵ_i are the wavenumber and permittivity of region i, respectively. ϖ is the angular frequency, and the permeability of all regions is equal to μ_o of free space. σ is the conductivity of the inner conductor, and $\tan\delta_{\mathbf{i}}$ is the loss tangent of the dielectric materials in regions II and III. I_n and K_n denote the modified Bessel functions. $A_{mn}^{(i)}$, $B_{mn}^{(i)}$, $C_{mn}^{(i)}$, and $D_{mn}^{(i)}$ are unknown coefficients to be determined.

In each region i using (3), the electromagnetic fields can be expressed as

$$E^{(i)} = \nabla\nabla\cdot\Pi_e^{(i)} + k_i^2\Pi_e^{(i)} - j\varpi\mu_o\nabla\times\Pi_m^{(i)}$$
$$H^{(i)} = \nabla\nabla\cdot\Pi_m^{(i)} + k_i^2\Pi_m^{(i)} + j\varpi\epsilon_i\nabla\times\Pi_e^{(i)}, \qquad i = \mathrm{I}, \mathrm{II}, \mathrm{III}, \mathrm{IV}. \tag{4}$$

C. Application of Boundary Conditions

To solve the problem, boundary conditions between regions are used. First, utilizing the orthogonality properties for the tangential electric fields E_ϕ and E_z in region II at $\rho = b$, we obtain

$$P_{11}A_{mn}^{(2)} + P_{12}B_{mn}^{(2)} + P_{13}C_{mn}^{(2)} + P_{14}D_{mn}^{(2)} = F(m, n) \tag{5}$$
$$P_{21}A_{mn}^{(2)} + P_{22}B_{mn}^{(2)} = G(m, n) \tag{6}$$

where

$$P_{11} = n\alpha_m I_n(\beta_m^{(2)} b) \qquad P_{12} = n\alpha_m K_n(\beta_m^{(2)} b)$$
$$P_{13} = jb\varpi\mu_o\beta_m^{(2)} I_n'(\beta_m^{(2)} b) \qquad P_{14} = jb\varpi\mu_o\beta_m^{(2)} K_n'(\beta_m^{(2)} b)$$
$$P_{21} = -\beta_m^{(2)^2} I_n(\beta_m^{(2)} b) \qquad P_{22} = -\beta_m^{(2)^2} K_n(\beta_m^{(2)} b)$$

where the prime indicates derivation with respect to the argument of the modified Bessel function, and

$$F(m, n) = \frac{b}{2\pi p}\int_0^p \int_{-\pi}^{\pi} E_{\phi|\rho=b} e^{-jn\phi} e^{j\alpha_m z}\, d\phi\, dz \quad (7)$$

$$G(m, n) = \frac{1}{2\pi p}\int_0^p \int_{-\pi}^{\pi} E_{z|\rho=b} e^{-jn\phi} e^{j\alpha_m z}\, d\phi\, dz. \quad (8)$$

In (7) and (8), $E_{\phi|\rho=b}$ and $E_{z|\rho=b}$ are the tangential electric fields in the slots.

Second, the condition that the tangential fields E_z and H_z in regions I and II must be continuous at $\rho = a$ results in

$$A_{mn}^{(1)} = \frac{B_m^{(2)^2}}{\beta_m^{(1)^2} I_n(\beta_m^{(1)} a)}[I_n(\beta_m^{(2)} a) A_{mn}^{(2)} + K_n(\beta_m^{(2)} a) B_{mn}^{(2)}] \quad (9)$$

$$C_{mn}^{(1)} = \frac{B_m^{(2)^2}}{\beta_m^{(1)^2} I_n(\beta_m^{(1)} a)}[I_n(\beta_m^{(2)} a) C_{mn}^{(2)} + K_n(\beta_m^{(2)} a) D_{mn}^{(2)}]. \quad (10)$$

Since the fields are finite in region I, $B_{mn}^{(1)}$ and $D_{mn}^{(1)}$ must be zero.

Third, using (9) and (10), and the continuity of E_ϕ and H_ϕ in regions I and II at $\rho = a$, we obtain

$$P_{31} A_{mn}^{(2)} + P_{32} B_{mn}^{(2)} + P_{33} C_{mn}^{(2)} + P_{34} D_{mn}^{(2)} = 0 \quad (11)$$
$$P_{41} A_{mn}^{(2)} + P_{42} B_{mn}^{(2)} + P_{43} C_{mn}^{(2)} + P_{44} D_{mn}^{(2)} = 0 \quad (12)$$

where

$$P_{31} = n\alpha_m\left(\frac{\beta_m^{(2)^2}}{\beta_m^{(1)^2}} - 1\right) I_n(\beta_m^{(2)} a)$$
$$P_{32} = n\alpha_m\left(\frac{\beta_m^{(2)^2}}{\beta_m^{(1)^2}} - 1\right) K_n(\beta_m^{(2)} a)$$
$$P_{33} = j\varpi\mu_o a\left[\frac{\beta_m^{(2)^2}}{\beta_m^{(1)}}\frac{I_n'(\beta_m^{(1)} a)}{I_n(\beta_m^{(1)} a)} I_n(\beta_m^{(2)} a) - \beta_m^{(2)} I_n'(\beta_m^{(2)} a)\right]$$
$$P_{34} = j\varpi\mu_o a\left[\frac{\beta_m^{(2)^2}}{\beta_m^{(1)}}\frac{I_n'(\beta_m^{(1)} a)}{I_n(\beta_m^{(1)} a)} K_n(\beta_m^{(2)} a) - \beta_m^{(2)} K_n'(\beta_m^{(2)} a)\right]$$
$$P_{41} = -j\varpi a\left[\epsilon_1\frac{\beta_m^{(2)^2}}{\beta_m^{(1)}}\frac{I_n'(\beta_m^{(1)} a)}{I_n(\beta_m^{(1)} a)} I_n(\beta_m^{(2)} a) - \epsilon_2\beta_m^{(2)} I_n'(\beta_m^{(2)} a)\right]$$
$$P_{42} = -j\varpi a\left[\epsilon_1\frac{\beta_m^{(2)^2}}{\beta_m^{(1)}}\frac{I_n'(\beta_m^{(1)} a)}{I_n(\beta_m^{(1)} a)} K_n(\beta_m^{(2)} a) - \epsilon_2\beta_m^{(2)} K_n'(\beta_m^{(2)} a)\right]$$
$$P_{43} = n\alpha_m\left(\frac{\beta_m^{(2)^2}}{\beta_m^{(1)^2}} - 1\right) I_n(\beta_m^{(2)} a)$$
$$P_{44} = n\alpha_m\left(\frac{\beta_m^{(2)^2}}{\beta_m^{(1)^2}} - 1\right) K_n(\beta_m^{(2)} a).$$

From (5), (6), (11), and (12), we obtain four equations with four unknown coefficients $A_{mn}^{(2)}$, $B_{mn}^{(2)}$, $C_{mn}^{(2)}$, and $D_{mn}^{(2)}$. These equations can be expressed in matrix form as follows:

$$\begin{vmatrix} A^{(2)} \\ B^{(2)} \\ C^{(2)} \\ D^{(2)} \end{vmatrix} = \begin{bmatrix} P_{11} & \cdot & \cdot & P_{14} \\ \cdot & & & \\ \cdot & & & \\ P_{41} & \cdot & \cdot & P_{44} \end{bmatrix}^{-1} \begin{vmatrix} F \\ G \\ 0 \\ 0 \end{vmatrix} = \begin{bmatrix} \tilde{P}_{11} & \cdot & \cdot & \tilde{P}_{14} \\ \cdot & & & \\ \cdot & & & \\ \tilde{P}_{41} & \cdot & \cdot & \tilde{P}_{44} \end{bmatrix} \begin{vmatrix} F \\ G \\ 0 \\ 0 \end{vmatrix}. \quad (13)$$

If the fundamental propagation constant α_o and the tangential electric fields in the slots are known, (13) can be solved to obtain the four unknown coefficients. From (9) and (10), $A_{mn}^{(1)}$ and $C_{mn}^{(1)}$ can also be calculated. Thus, the field distributions in regions I and II are represented completely.

For the case of regions III and IV, the above procedures can be applied in the exactly same manner, replacing region I by region IV, region II by region III, and $\rho = a$ by $\rho = c$. Thus, we present the following results.

As in (5) and (6)

$$Q_{11} A_{mn}^{(3)} + Q_{12} B_{mn}^{(3)} + Q_{13} C_{mn}^{(3)} + Q_{14} D_{mn}^{(3)} = F(m, n) \quad (14)$$
$$Q_{21} A_{mn}^{(3)} + Q_{22} B_{mn}^{(3)} = G(m, n) \quad (15)$$

where

$$Q_{11} = n\alpha_m I_n(\beta_m^{(3)} b) \qquad Q_{12} = n\alpha_m K_n(\beta_m^{(3)} b)$$
$$Q_{13} = jb\varpi\mu_o\beta_m^{(3)} I_n'(\beta_m^{(3)} b) \qquad Q_{14} = jb\varpi\mu_o\beta_m^{(3)} K_n'(\beta_m^{(3)} b)$$
$$Q_{21} = -\beta_m^{(3)^2} I_n(\beta_m^{(3)} b) \qquad Q_{22} = -\beta_m^{(3)^2} K_n(\beta_m^{(3)} b).$$

As in (9) and (10)

$$B_{mn}^{(4)} = \frac{\beta_m^{(3)^2}}{\beta_m^{(4)^2} K_n(\beta_m^{(4)} c)}[I_n(\beta_m^{(3)} c) A_{mn}^{(3)} + K_n(\beta_m^{(3)} c) B_{mn}^{(3)}] \quad (16)$$

$$D_{mn}^{(4)} = \frac{\beta_m^{(3)^2}}{\beta_m^{(4)^2} K_n(\beta_m^{(4)} c)}[I_n(\beta_m^{(3)} c) C_{mn}^{(3)} + K_n(\beta_m^{(3)} c) D_{mn}^{(3)}]. \quad (17)$$

Since the fields at $\rho = \infty$ are finite, $A_{mn}^{(4)}$ and $C_{mn}^{(4)}$ must be zero.

As in (11) and (12)

$$Q_{31} A_{mn}^{(3)} + Q_{32} B_{mn}^{(3)} + Q_{33} C_{mn}^{(3)} + Q_{34} D_{mn}^{(3)} = 0 \quad (18)$$
$$Q_{41} A_{mn}^{(3)} + Q_{42} B_{mn}^{(3)} + Q_{43} C_{mn}^{(3)} + Q_{44} D_{mn}^{(3)} = 0 \quad (19)$$

where

$$Q_{31} = n\alpha_m\left(\frac{\beta_m^{(3)^2}}{\beta_m^{(4)^2}} - 1\right) I_n(\beta_m^{(3)}c)$$

$$Q_{32} = n\alpha_m\left(\frac{\beta_m^{(3)^2}}{\beta_m^{(4)^2}} - 1\right) K_n(\beta_m^{(3)}c)$$

$$Q_{33} = j\varpi\mu_o c\left[\frac{\beta_m^{(3)^2}}{\beta_m^{(4)}}\frac{K_n'(\beta_m^{(4)}c)}{K_n(\beta_m^{(4)}c)} I_n(\beta_m^{(3)}c) - \beta_m^{(3)} I_n'(\beta_m^{(3)}c)\right]$$

$$Q_{34} = j\varpi\mu_o c\left[\frac{\beta_m^{(3)^2}}{\beta_m^{(4)}}\frac{K_n'(\beta_m^{(4)}c)}{K_n(\beta_m^{(4)}c)} K_n(\beta_m^{(3)}c) - \beta_m^{(3)} K_n'(\beta_m^{(3)}c)\right]$$

$$Q_{41} = -j\varpi c\left[\epsilon_4\frac{\beta_m^{(3)^2}}{\beta_m^{(4)}}\frac{K_n'(\beta_m^{(4)}c)}{K_n(\beta_m^{(4)}c)} I_n(\beta_m^{(3)}c) - \epsilon_3\beta_m^{(3)} I_n'(\beta_m^{(3)}c)\right]$$

$$Q_{42} = -j\varpi c\left[\epsilon_4\frac{\beta_m^{(3)^2}}{\beta_m^{(4)}}\frac{K_n'(\beta_m^{(4)}c)}{K_n(\beta_m^{(4)}c)} K_n(\beta_m^{(3)}c) - \epsilon_3\beta_m^{(3)} K_n'(\beta_m^{(3)}c)\right]$$

$$Q_{43} = n\alpha_m\left(\frac{\beta_m^{(3)^2}}{\beta_m^{(4)^2}} - 1\right) I_n(\beta_m^{(3)}c)$$

$$Q_{44} = n\alpha_m\left(\frac{\beta_m^{(3)^2}}{\beta_m^{(4)^2}} - 1\right) K_n(\beta_m^{(3)}c).$$

From (14), (15), (18), and (19), we obtain similar result as in (13):

$$\begin{vmatrix} A^{(3)} \\ B^{(3)} \\ C^{(3)} \\ D^{(3)} \end{vmatrix} = \begin{bmatrix} Q_{11} & \cdot & \cdot & Q_{14} \\ \cdot & & & \\ \cdot & & & \\ Q_{41} & \cdot & \cdot & Q_{44} \end{bmatrix}^{-1} \begin{vmatrix} F \\ G \\ 0 \\ 0 \end{vmatrix} = \begin{bmatrix} \tilde{Q}_{11} & \cdot & \cdot & \tilde{Q}_{14} \\ \cdot & & & \\ \cdot & & & \\ \tilde{Q}_{41} & \cdot & \cdot & \tilde{Q}_{44} \end{bmatrix} \begin{vmatrix} F \\ G \\ 0 \\ 0 \end{vmatrix}. \tag{20}$$

D. Electric Fields in the Slots

To represent the fields in the slots, a new coordinate system is introduced in Fig. 2. The slots are sufficiently narrow so that it is reasonable to assume that for each slot

$$E_\zeta^s = 0$$

$$E_\xi^s(\zeta, \xi) = \delta(\xi - \Delta_{\xi_s})\sum_{i=1}^{I} A_i^s \sin\left[i\pi(\zeta - \Delta_{\zeta_s} + l_s/2)/l_s\right] \cdot e^{-j\alpha_0 z}, \qquad s = 1, 2, \cdots, S \tag{21}$$

where A_i^s's are to be determined by Galerkin's method and I is the number of basis functions. Δ_{ζ_s} and Δ_{ξ_s} are the displacements of the sth slot in ζ and ξ directions, respectively.

E_ξ^s in (21) is divided into two vector components in the original coordinate system:

$$E_\phi^s = -\cos\theta_s\delta(\xi - \Delta_{\xi_s}) \cdot \sum_{i=1}^{I} A_i^s \sin\left[i\pi(\zeta - \Delta_{\zeta_s} + l_s/2)/l_s\right] e^{-j\alpha_0 z} \tag{22}$$

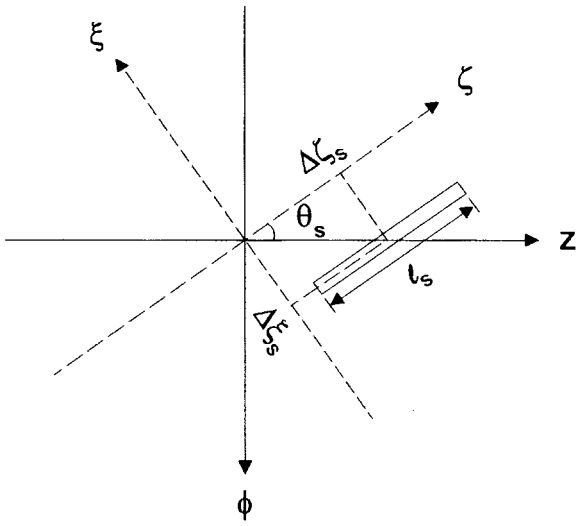

Fig. 2. New coordinate system for inclined slot.

$$E_z^s = -\sin\theta_s\delta(\xi - \Delta_{\xi_s}) \cdot \sum_{i=1}^{I} A_i^s \sin\left[i\pi(\zeta - \Delta_{\zeta_s} + l_s/2)/l_s\right] e^{-j\alpha_0 z}, \qquad s = 1, 2, \cdots, S. \tag{23}$$

Using (22) and (23), (7) and (8) can be rewritten as

$$F(m, n) = b\sum_{s=1}^{S}\cos\theta_s\sum_{i=1}^{I} A_i^s h^s(i, m, n) \tag{24}$$

$$G(m, n) = \sum_{s=1}^{S}\sin\theta_s\sum_{i=1}^{I} A_i^s h^s(i, m, n) \tag{25}$$

where

$$h^s(i, m, n) = -\frac{1}{2\pi p}\int_0^p\int_{-\pi}^{\pi}\delta(\xi - \Delta_{\xi_s})\sin\left[i\pi(\zeta - \Delta_{\zeta_s} + l_s/2)/l_s\right] \cdot e^{-j\alpha_0 z}e^{-jn\phi}e^{j\alpha_m z}\, d\phi\, dz.$$

E. Determination of Propagation Constant

Now we are in the position to match the tangential magnetic fields in the slots between regions II and III. For each slot in a pitch

$$H_{\zeta|\rho=b}^{s(2)} = H_{\zeta|\rho=b}^{s(3)}, \qquad s = 1, 2, \cdots, S. \tag{26}$$

In the original coordinate system, (26) is given by

$$-\sin\theta_s(H_{\phi|\rho=b}^{s(2)} - H_{\phi|\rho=b}^{s(3)}) + \cos\theta_s(H_{z|\rho=b}^{s(2)} - H_{z|\rho=b}^{s(3)}) = 0, \qquad s = 1, 2, \cdots, S. \tag{27}$$

H_ϕ^s and H_z^s in (27) are obtained from (4) where their coefficients are from (13) and (20). Applying Galerkin's method in (27) we obtain (28), shown at the bottom of the following page.

To obtain a nonvanishing solution of matrix $[A]$ in (28), the determinant of matrix $[M]$ must be zero, i.e.,

$$\det[M] = 0. \tag{29}$$

The determinant of matrix $[M]$ has only one unknown variable α_o so that the propagation constant can be obtained by solving (29). Finally, the field distributions in all regions can be calculated using (4), (13), and (20).

IV. Numerical Results

A. General Description

The determinant of matrix $[M]$ in (29) is a complex-valued nonlinear equation. In solving the equation, the small argument approximations of I_n and K_n in (3) cannot be used because the arguments range from $-\infty$ to ∞ as functions of β_m. In this paper, the recurrence relations in [18] are used to obtain I_n and K_n. To find the fundamental propagation constant α_o, a complex-root-finding Muller method is used. Parameters for the numerical calculations are listed in Table I, which are usually accepted for the commercially available LCX's. p, the pitch, is fixed as 2 m. The lengths of all slots are equal as l, and the angles have sinusoidal distribution given by

$$\theta_n = \theta_{\max} \times \sin\left(\frac{2\pi}{N}n\right), \qquad n = 1, \cdots, N-1 \tag{30}$$

where $\theta_{\max}$ is the maximum value of the slot angles, and N is $S+2$.

All slots are placed in equal space of p/N. Among these, the $N/2$th (N: even) slot with $\theta_{N/2} = 0$ is removed because it does not contribute to leaky wave properties. Hence, there are S slots per pitch. Fig. 3 shows the slot arrangements of LCX's analyzed in this paper. Most of the analysis will be focused on the 14-slot LCX, the latest version.

B. Propagation Constant

It is possible that both the bifilar mode and the monofilar mode simultaneously exist, as in RCX. However, in this paper only the bifilar mode is considered because communication applications for LCX utilize only the bifilar mode.

To verify the theory in Section III, the analysis has been applied to single-slot structures considered in [11] and [12]. In [11], all cases are lossless, and the sheath outside the outer conductor does not exist. The single-slot coaxial cable in [12] is buried under lossy ground. In both cases, only the bifilar mode has been compared, and the results are listed in Table II. The same situation as in [11] is obtained by assuming that all

$$\begin{vmatrix} {}_{11}M_{11} & \cdots & {}_{11}M_{1I} & \cdots & \cdots & {}_{11}M_{S1} & \cdots & {}_{11}M_{SI} \\ {}_{12}M_{11} & \cdots & {}_{12}M_{1I} & \cdots & \cdots & {}_{12}M_{S1} & \cdots & {}_{12}M_{SI} \\ \vdots & & & & & & & \\ {}_{1I}M_{11} & \cdots & {}_{1I}M_{1I} & \cdots & \cdots & {}_{1I}M_{S1} & \cdots & {}_{1I}M_{SI} \\ {}_{21}M_{11} & \cdots & {}_{21}M_{1I} & \cdots & \cdots & {}_{21}M_{S1} & \cdots & {}_{21}M_{SI} \\ \vdots & & & & & & & \\ \vdots & & & & & & & \\ {}_{2I}M_{11} & \cdots & {}_{2I}M_{1I} & \cdots & \cdots & {}_{2I}M_{S1} & \cdots & {}_{2I}M_{SI} \\ \vdots & & & & & & & \\ \vdots & & & & & & & \\ \vdots & & & & & & & \\ \vdots & & & & & & & \\ {}_{SI}M_{11} & \cdots & {}_{SI}M_{1I} & \cdots & \cdots & {}_{SI}M_{S1} & \cdots & {}_{SI}M_{SI} \end{vmatrix} \begin{vmatrix} A_1^1 \\ \vdots \\ A_I^1 \\ \vdots \\ \vdots \\ \vdots \\ \vdots \\ \vdots \\ A_1^S \\ \vdots \\ A_I^S \end{vmatrix} = 0 \tag{28}$$

where

$$\begin{aligned}
{}_{si}M_{tj} &= -\sin\theta_s(V_{ij}^{st} + W_{ij}^{st}) + \cos\theta_s(X_{ij}^{st} + Y_{ij}^{st}), \qquad s, t = 1, 2, \cdots, S \quad i, j = 1, 2, \cdots, I \\
V_{ij}^{st} &= b\cos\theta_t \sum_m \sum_n \{-j\omega[\epsilon_2\beta_m^{(2)}(\tilde{P}_{11}I_n'(\beta_m^{(2)}b) + \tilde{P}_{21}K_n'(\beta_m^{(2)}b)) - \epsilon_3\beta_m^{(3)}(\tilde{Q}_{11}I_n'(\beta_m^{(3)}b) + \tilde{Q}_{21}K_n'(\beta_m^{(3)}b))] \\
&\qquad + \frac{n\alpha_m}{b}[(\tilde{P}_{31}I_n(\beta_m^{(2)}b) + \tilde{P}_{41}K_n(\beta_m^{(2)}b)) - (\tilde{Q}_{31}I_n(\beta_m^{(3)}b) + \tilde{Q}_{41}K_n(\beta_m^{(3)}b))]\} \\
&\quad \cdot h^s(i, m, n) \cdot h^t(j, m, n) \\
W_{ij}^{st} &= \sin\theta_t \sum_m \sum_n \{-j\omega[\epsilon_2\beta_m^{(2)}(\tilde{P}_{12}I_n'(\beta_m^{(2)}b) + \tilde{P}_{22}K_n'(\beta_m^{(2)}b)) - \epsilon_3\beta_m^{(3)}(\tilde{Q}_{12}I_n'(\beta_m^{(3)}b) + \tilde{Q}_{22}K_n'(\beta_m^{(3)}b))] \\
&\qquad + \frac{n\alpha_m}{b}[(\tilde{P}_{32}I_n(\beta_m^{(2)}b) + \tilde{P}_{42}K_n(\beta_m^{(2)}b)) - (\tilde{Q}_{32}I_n(\beta_m^{(3)}b) + \tilde{Q}_{42}K_n(\beta_m^{(3)}b))]\} \\
&\quad \cdot h^s(i, m, n) \cdot h^t(j, m, n) \\
X_{ij}^{st} &= -b\cos\theta_t \sum_m \sum_n [\beta_m^{(2)^2}(\tilde{P}_{31}I_n(\beta_m^{(2)}b) + \tilde{P}_{41}K_n(\beta_m^{(2)}b)) - \beta_m^{(3)^2}(\tilde{Q}_{31}I_n(\beta_m^{(3)}b) + \tilde{Q}_{41}K_n(\beta_m^{(3)}b))] \\
&\quad \cdot h^s(i, m, n) \cdot h^t(j, m, n) \\
Y_{ij}^{st} &= -\sin\theta_t \sum_m \sum_n [\beta_m^{(2)^2}(\tilde{P}_{32}I_n(\beta_m^{(2)}b) + \tilde{P}_{42}K_n(\beta_m^{(2)}b)) - \beta_m^{(3)^2}(\tilde{Q}_{32}I_n(\beta_m^{(3)}b) + \tilde{Q}_{42}K_n(\beta_m^{(3)}b))] \\
&\quad \cdot h^s(i, m, n) \cdot h^t(j, m, n)
\end{aligned}$$

TABLE I
PARAMETERS OF LCX FOR NUMERICAL CALCULATIONS ($\epsilon_i' = \epsilon_r^{(i)} \cdot \epsilon_o$)

inner conductor	material	aluminium	outer conductor	material	perfect conductor
	a(mm)	8.65		b(mm)	21
	σ (mhos/m)	3.82×10^7		σ (mhos/m)	∞
dielectric material between conductors	material	poly ethylene	sheath	material	poly ethylene
	b(mm)	21		c(mm)	25
	$\varepsilon_r^{(2)}$	1.2		$\varepsilon_r^{(3)}$	4.0
	$\tan\delta_2$	10^{-4}		$\tan\delta_3$	10^{-3}

TABLE II
COMPARISONS OF THE PROPAGATION CONSTANTS OF SINGLE-SLOT COAXIAL CABLES

angle	frequency (MHz)	normalized phase constant			attenuation constant (dB/Km)	
		this paper	ref. [11]	ref. [12]	this paper	ref. [12]
ϕ_o = 45°	10	1.427	1.427	-	-	-
	100	1.427	1.427	-	-	-
	1000	1.427	1.428	-	-	-
ϕ_o = 180°	10	1.628	1.659	-	-	-
	100	1.633	1.663	-	-	-
	1000	1.675	1.710	-	-	-
ϕ_o = 45°	100	0.785	-	0.785	17.92	17.55

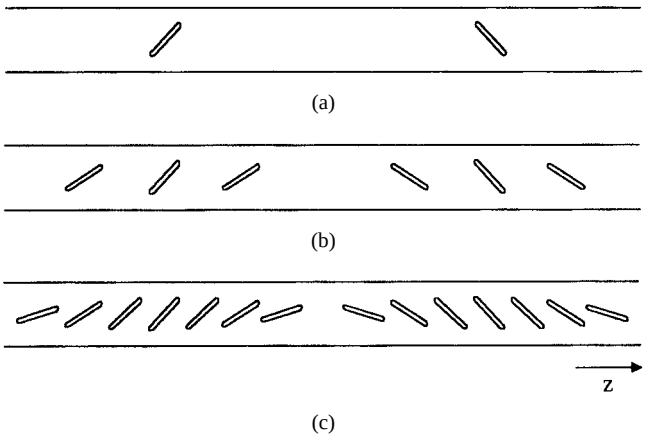

Fig. 3. Slot arrangements for numerical calculations. (a) Two-slot. (b) Six-slot. (c) 14-slot.

materials are lossless, and $\epsilon_r^{(3)}$ is equal to 1 in Table I. The results agree well in each other for $\phi_o = 45°$. The difference between them for $\phi_o = 180°$ is less than 2%, and the steeply increasing behavior with increasing frequency is observed in both results. Although the environments around the cable in [12] are different from this paper, the results are in good agreement because the bifilar mode has most of its energy inside the cable, thus rarely affected by the outer space.

The convergence of the propagation constant α_o has been checked as the second verification. There are three parameters (i, m, n) determining the convergence of the propagation constant. It has been found that the number of n determines most of the convergence. Fig. 4 shows the convergence of a 14-slot LCX at 900 MHz as a function of n, where n means $[-n, n]$ in (3). Both the phase constant α_o' and the attenuation constant α_o'' converge well, where α_o' is normalized by the free-space wavenumber k_o, and α_o'' is expressed in decibels/kilometers. $I = 1$ and $m = [-14, 14]$ are good enough so that they will be maintained throughout the paper. It must be also noted that an order of 10^{-10} of convergence rate is required to obtain the converged field distributions, needing more than $n = 300$. For less slots per pitch and lower frequency, less n's are needed. Fig. 5(a) shows the normalized phase constant as a function of the number of slots per pitch and frequency. As expected, more slots cause larger phase constant, meaning more perturbation of the TEM wave inside the coaxial cable. The attenuation constants in decibels/kilometers do not vary considerably in all cases considered in this paper, so they are not distinguished in

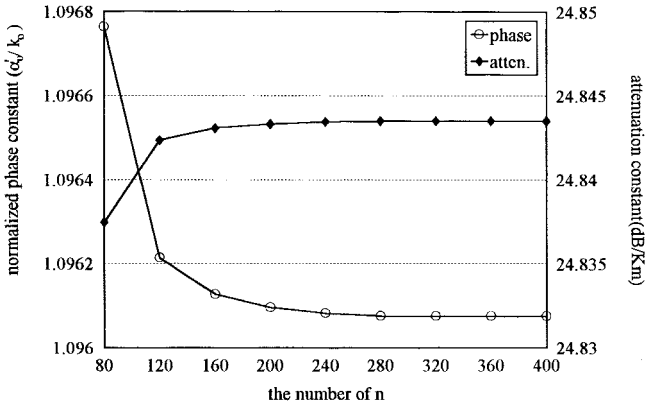

Fig. 4. Convergence of the propagation constant α_o at 900 MHz ($S = 14$, $\theta_{\max} = 24°$, $l = 100$ mm).

a convenient form of figure. Hence, all the results of the attenuation constant are provided in Tables III–V. In Table III, more slots exhibit less attenuation for the same frequency, which seems to be somewhat contradictory. The reason is as follows. The attenuation is categorized into two. One is the conductor and dielectric loss of the surface wave, and the other is the radiation loss due to the leaky wave. In LCX, leakage is usually very small so that most of the transmission loss is the conductor and dielectric loss especially of the fundamental modes $(m = 0)$. In a practical situation, the environment around LCX is not perfectly lossless, rather randomly distributed lossy media like concrete walls or posts, which is a case-by-case problem that cannot be considered analytically. In our case, the surface wave inside the cable attenuates through the lossy conductor and dielectric material, but the surface wave outside the cable does not experience loss as in the practical case. From Table III, more slots result in less transmission loss, meaning that more slots provide more energy into the lossless free space outside the cable, consistent with more perturbation of the inner TEM wave by more slots in Fig. 5(a). This situation will be further investigated later in Section IV-D. Fig. 5(b) and (c) is for various slot angles and lengths. The slot angle θ in degree, hereafter, means the maximum slot angle $\theta_{\max}$ in (30). As expected, larger angle and longer length cause more perturbation of the inner TEM wave. The transmission losses in Tables IV and V can be considered as stated above. One exception is observed for $\theta = 48°$ at 900 MHz in Table IV. The transmission loss for $\theta = 48°$ is larger than for smaller angles. In this case, the second loss term, the radiation loss due to leaky wave, is the main cause. The leaky wave contributes to the transmission loss even in the lossless free space. As will be seen in Section IV-C, the amount of leaky wave for $\theta = 48°$ is much larger than for other cases at 900 MHz.

C. Coupling Loss

Coupling loss is defined as usual:

$$\text{coupling loss (dB)} = -10 \log \frac{P_r}{P_t} \tag{31}$$

where P_t is the power transmitted inside the cable and P_r is the power received from LCX.

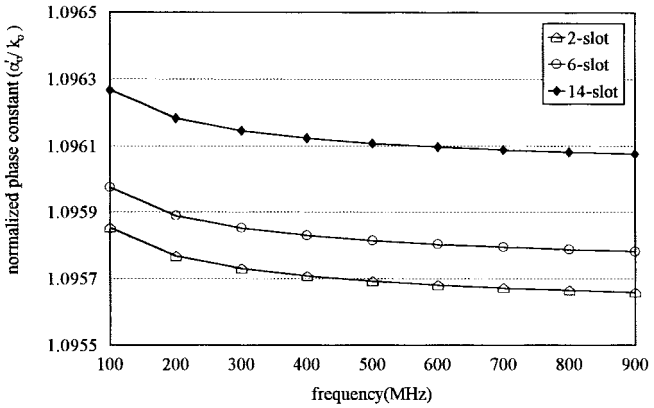

(a)

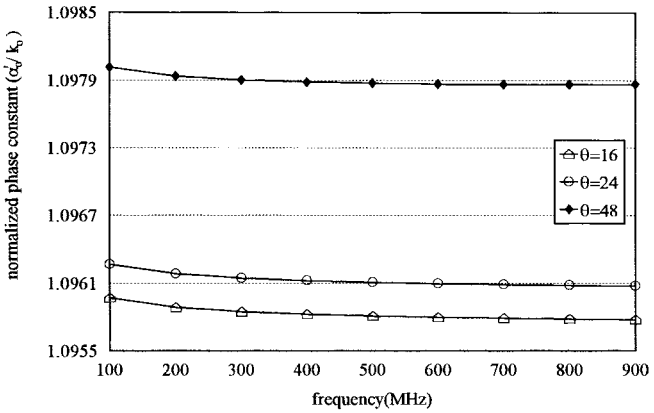

(b)

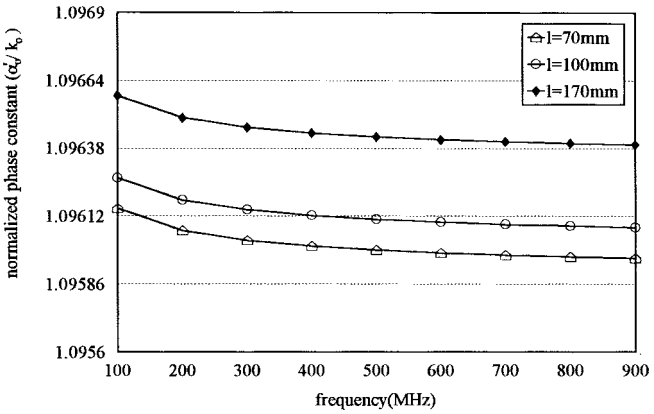

(c)

Fig. 5. (a) Normalized phase constant as a function of the number of slots per pitch and frequency ($\theta_{\max} = 24°$, $l = 100$ mm). (b) Normalized phase constant as a function of slot angle and frequency ($S = 14$, $l = 100$ mm). (c) Normalized phase constant as a function of slot length and frequency ($S = 14$, $\theta_{\max} = 24°$).

The coupling loss of LCX is measured facing slots along the cable with a standard half-wavelength dipole antenna separated from LCX by 1.5 m, as shown in Fig. 6. In this paper, for computational simplicity, the numerical results of coupling loss are obtained using infinitesimal dipole antenna instead of the standard half-wavelength dipole antenna. In (31), P_t is calculated from the fields in region II, and P_r is obtained from the Poynting vector reaching to the maximum effective aperture of the infinitesimal dipole antenna in free space.

TABLE III
ATTENUATION CONSTANT IN dB/km AS A FUNCTION OF THE NUMBER OF SLOTS PER PITCH AND FREQUENCY ($\theta_{\max} = 24°$, $l = 100$ mm)

the number of slots per pitch / frequency(MHz)	2-slot(S=2)	6-slot(S=6)	14-slot(S=14)
100	6.2869	6.2864	6.2852
300	12.1546	12.1539	12.1522
500	16.8158	16.8150	16.8130
700	20.9779	20.9770	20.9749
900	24.8467	24.8458	24.8435

TABLE IV
ATTENUATION CONSTANT IN dB/km AS A FUNCTION OF SLOT ANGLE AND FREQUENCY ($S = 14$, $l = 100$ mm)

slot angle / frequency(MHz)	$\theta = 16°$	$\theta = 24°$	$\theta = 48°$
100	6.2864	6.2852	6.2777
300	12.1540	12.1522	12.1408
500	16.8151	16.8130	16.8016
700	20.9771	20.9749	20.9686
900	24.8458	24.8435	24.8509

TABLE V
ATTENUATION CONSTANT IN dB/km AS A FUNCTION OF SLOT LENGTH AND FREQUENCY ($S = 14$, $\theta_{\max} = 24°$)

slot length / frequency(MHz)	l = 70mm	l = 100mm	l = 170mm
100	6.2857	6.2852	6.2839
300	12.1529	12.1522	12.1502
500	16.8139	16.8130	16.8106
700	20.9759	20.9749	20.9722
900	24.8447	24.8435	24.8405

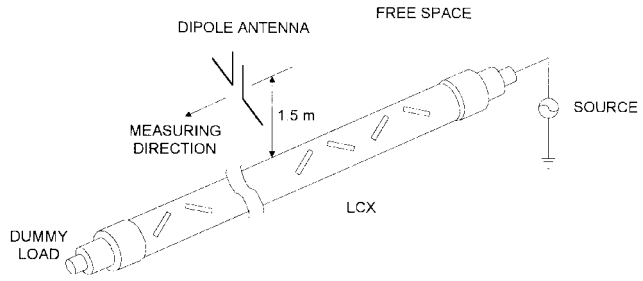

Fig. 6. Measurement of coupling loss for LCX.

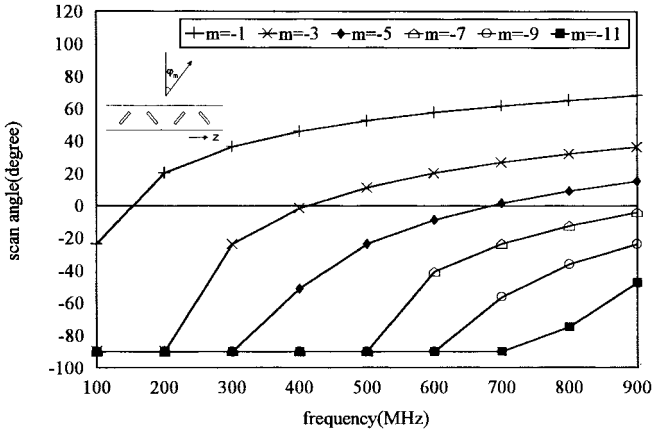

(a)

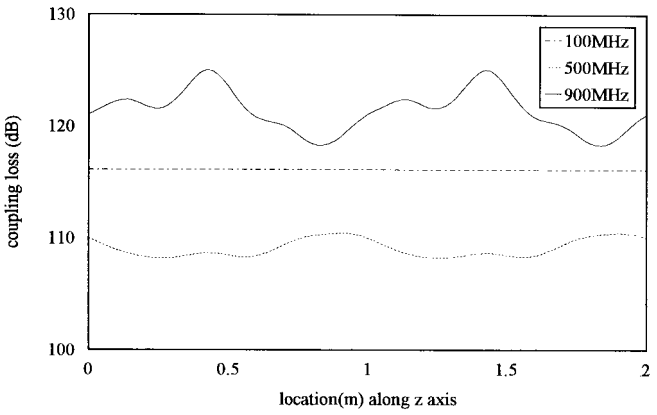

(b)

Fig. 7. (a) Beam directions of spatial harmonics versus frequency ($S = 14$, $\theta_{\max} = 24°$, $l = 100$ mm). (b) Coupling loss along the cable as a function of frequency ($S = 2$, $\theta_{\max} = 24°$, $l = 100$ mm).

To consider the interfering effect of many coupling modes it is necessary to define the beam direction of the mth spatial harmonic calculated from broadside as

$$\sin\varphi_m = \frac{\mathrm{Re}[\alpha_m]}{k_o}. \tag{32}$$

Fig. 7(a) shows the beam directions of the spatial harmonics versus frequency, where we include only the odd spatial harmonics for clear view. At 100 MHz only $m = -1$ spatial harmonic radiates ($\varphi_{-1} = -20°$), and other harmonics remain as surface waves ($\varphi_m \cong -90°$). As frequency becomes higher, $m = -2$ begins to radiate, then $m = -3$, and so on, arising from backfire ($\varphi_m \cong -90°$) toward endfire ($\varphi_m \cong 90°$). Since at lower frequency only $m = -1$ leaky wave exists, coupling loss is flat along the cable. However, at higher frequency leaky waves of the higher order spatial harmonics interfere with the desired $m = -1$, thus causing the fluctuation of the coupling loss. For two-slot LCX, shown in Fig. 7(b), the coupling loss is shown to have deeper fluctuation at higher frequency, limiting the broad-band capability of the two-slot LCX.

The fluctuation depth of the coupling loss can be reduced by placing more slots per pitch, as explained in Section II. Fig. 8(a) illustrates this principle at 900 MHz. As the number of slots is increased, the coupling loss becomes flat, producing more leaky wave. This result shows the reason why the

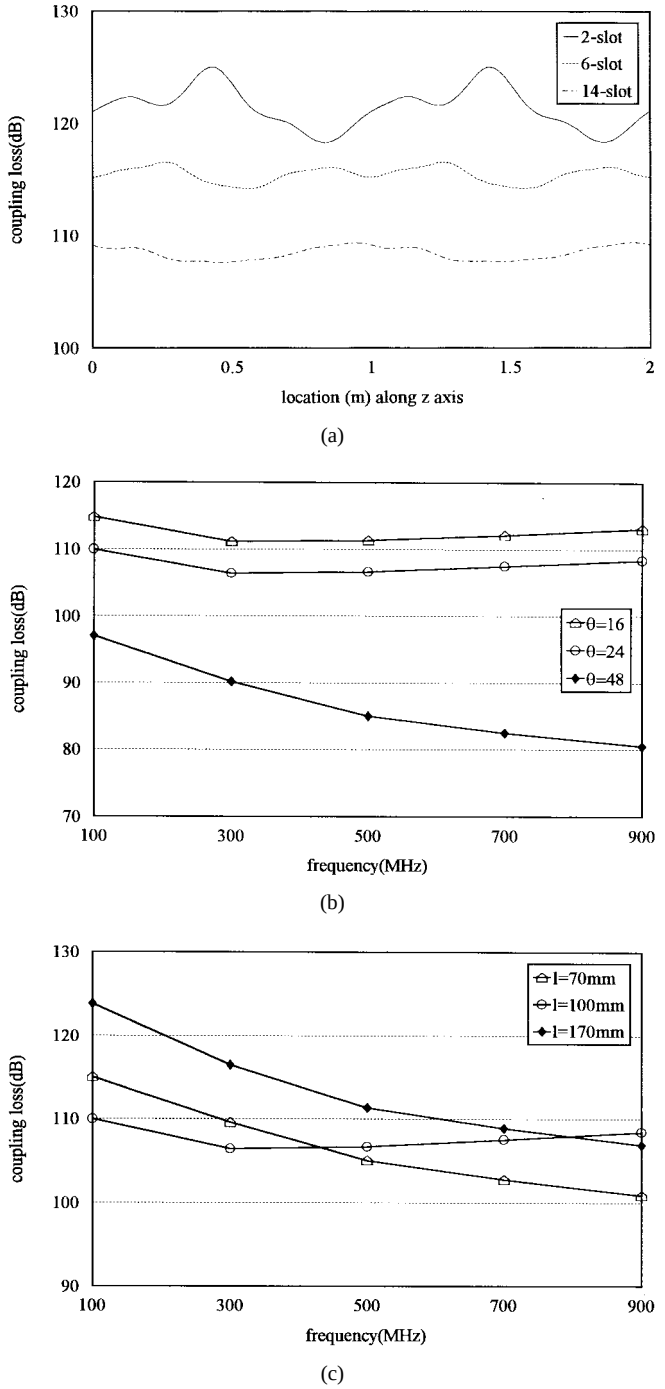

Fig. 8. (a) Coupling loss along the cable at 900 MHz as a function of the number of slots per pitch ($\theta_{\max} = 24^\circ$, $l = 100$ mm). (b) Coupling loss as a function of slot angle and frequency ($S = 14$, $l = 100$ mm). (c) Coupling loss as a function of slot length and frequency ($S = 14$, $\theta_{\max} = 24^\circ$).

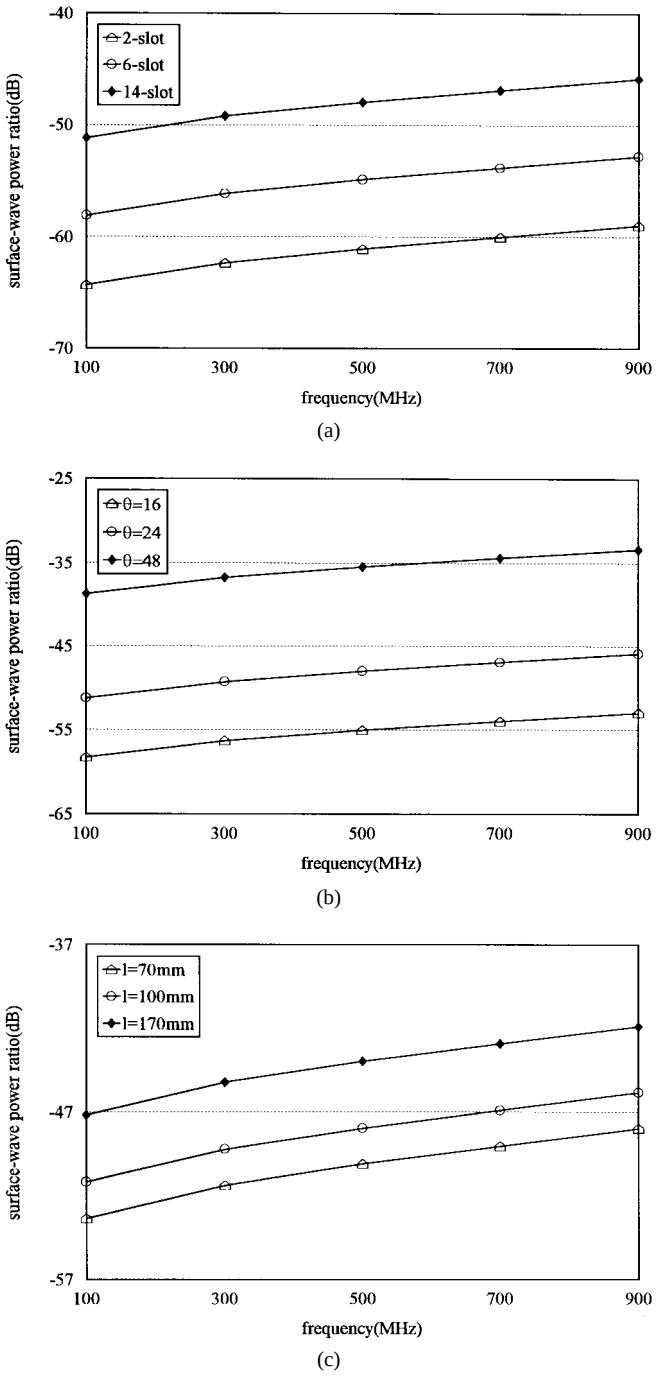

Fig. 9. (a) Surface wave power ratio as a function of the number of slots per pitch and frequency ($\theta_{\max} = 24^\circ$, $l = 100$ mm). (b) Surface wave power ratio as a function of slot angle and frequency ($S = 14$, $l = 100$ mm). (c) Surface wave power ratio as a function of slot length and frequency ($S = 14$, $\theta_{\max} = 24^\circ$).

latest LCX has more slots for its broad-band applications. Fig. 8(b) and (c) illustrates the coupling loss of 14-slot LCX for various slot angles and lengths. As expected, larger angle produces more leaky wave, thus more coupling loss. The LCX, however, exhibits nonuniform behavior with respect to the slot lengths. The frequency response of the coupling loss is more or less irregular depending on the slot lengths. In practical applications, large variation of coupling loss with frequency is not recommended. For a fixed slot angle, one needs to find a near-optimum slot length that provides flat frequency response of the coupling loss.

D. The Effect of Surface Wave on the Transmission Loss

Practically, surface waves corresponding to $m \geq 0$ contribute to the coupling loss in the same complex manner as in RCX, though the amount is not usually significant. Since most of the power of LCX is transmitted through the fundamental mode, this third loss term must be considered in any way. Although the randomly distributed lossy media in

real situations cannot be analyzed theoretically, the problem can be tackled indirectly. The third loss term is proportional to the amount of the surface wave of the fundamental mode outside the cable, which can be obtained using the theory in Section III. To this end, surface-wave power ratio is defined as follows:

$$\text{surface wave power ratio (dB)} = 10\log\frac{P_s}{P_t} \qquad (33)$$

where P_t is the same as in (31) and P_s is the power of the fundamental mode transmitted along z-direction outside the cable.

The results are presented in Fig. 9(a)–(c). Since the surface wave attenuates very steeply far from the cable, P_s in (33) is enough to calculate inside the radius of 1.5 m from the cable. Broad-band applications require more slots, which in turn generate more surface wave outside the cable, as illustrated in Fig. 9(a). 14-slot LCX produces 20 times more surface wave than two-slot LCX. Fig. 9(b) and (c) show the results of 14-slot LCX for various slot angles and lengths. It is observed that larger angle and longer length produce more surface wave. Note that the surface wave power ratio is more sensitive to the slot angles than to the slot lengths. It must also be noted that more surface waves are distributed at higher frequency: about three times more at 900 MHz than at 100 MHz.

When large leaky energy is needed, it is important to select the slot arrangements that do not produce excessive surface wave outside the cable. Otherwise, the transmission loss can become very large at higher frequency because the surface wave outside the cable contributes high to the third loss term.

V. Conclusion

In this paper, LCX with multiangle multislot structure has been analyzed. Using the moment method, the propagation constant and coupling loss have been obtained for various slot configurations. The normalized phase constant has been used to observe the amount of perturbation of the TEM wave transmitted inside the coaxial cable. Larger slot angle and longer slot length produce more perturbation, which also occurs for more slots per pitch.

The coupling loss indicates the amount of leaky energy to couple with another antenna. At lower frequency, only $m = -1$ spatial harmonic radiates so that the coupling loss is flat along the cable. However, as frequency becomes higher more modes $(m \leq -1)$ radiate, and interfere with each other. In this case, the coupling loss fluctuates along the cable, limiting the broad-band capability of LCX. To overcome this, one must place more slots per pitch: as an example in Section IV-C, the fluctuation depth of 14-slot LCX is 1.7 dB, whereas it is 6.7 dB for two-slot LCX. It has also been observed that larger slot angle produces more leaky energy, but longer slot length does not necessarily result in larger leakage. For a fixed angle, there is a near-optimum slot length that gives uniform coupling loss in the broad-band range.

The characteristics of the surface wave have also been considered in this paper. It is important to know the surface wave properties for various parameters, since the surface wave outside the cable contributes to the transmission loss in the practical case. As expected, larger slot angle and longer slot length cause more surface wave outside the cable at higher frequency. Usually, the loss due to the conductor and dielectric material inside the cable consists of most of the transmission loss. However, in some cases of large slot angle or long slot length the loss due to the leaky wave and surface wave outside the cable can contribute highly to the transmission loss.

References

[1] P. P. Delogne and M. Safak, "Electromagnetic theory of the leaky coaxial cable," *Radio Electron. Eng.*, vol. 45, no. 5, pp. 233–240, May 1975.

[2] J. R. Wait and D. A. Hill, "Propagation along a braided coaxial cable in a circular tunnel," *IEEE Trans. Microwave Theory Tech.*, vol. MTT-23, pp. 401–405, May 1975.

[3] D. B. Seidel and J. R. Wait, "Transmission modes in a braided coaxial cable and coupling to a tunnel environment," *IEEE Trans. Microwave Theory Tech.*, vol. MTT-26, pp. 494–499, July 1978.

[4] J. R. Wait, "Electromagnetic theory of the loosely braided coaxial cable: Part I," *IEEE Trans. Microwave Theory Tech.*, vol. MTT-24, pp. 547–553, Sept. 1976.

[5] D. A. Hill and J. R. Wait, "Propagation along a coaxial cable with a helical shield," *IEEE Trans. Microwave Theory Tech.*, vol. MTT-28, pp. 84–89, Feb. 1980.

[6] V. H. Rumsey, "Travelling wave slot antennas," *J. Appl. Phys.*, vol. 24, no. 11, pp. 1358–1365, Nov. 1953.

[7] R. A. Hurd, "The modes of an axially slotted coaxial waveguide," *Radio Sci.*, vol. 14, no. 5, pp. 741–751, Sept.–Oct. 1979.

[8] P. P. Delogne and A. A. Laloux, "Theory of the slotted coaxial cable," *IEEE Trans. Microwave Theory Tech.*, vol. MTT-28, pp. 1102–1107, Oct. 1980.

[9] E. E. Hassan, "Field solution and propagation characteristics of monofilar–bifilar modes of axially slotted coaxial cable," *IEEE Trans. Microwave Theory Tech.*, vol. 37, pp. 553–557, Mar. 1989.

[10] J. R. Wait, "Electromagnetic field analysis for a coaxial cable with periodic slots," *IEEE Trans. Electromag. Compat.*, vol. EMC-19, pp. 7–13, Feb. 1977.

[11] D. A. Hill and J. R. Wait, "Electromagnetic characteristics of a coaxial cable with periodic slots," *IEEE Trans. Electromag. Compat.*, vol. EMC-22, pp. 303–307, Nov. 1980.

[12] J. H. Richmond, N. N. Wang, and H. B. Tran, "Propagation of surface waves on a buried coaxial cable with periodic slots," *IEEE Trans. Electromag. Compat.*, vol. EMC-23, pp. 139–146, Aug. 1981.

[13] T. Sako, S. Misawa, T. Naruse, H. Yasuhara, M. Oguchi, and T. Kato, "Leaky coaxial cable," *Fujikura Tech. Rev.*, pp. 26–39, 1974.

[14] N. Tago, H. Satani, Y. Miyamoto, and Y. Amano, "Design and characteristics of radiating pair cable," in *Int. Wire Cable Symp. Proc.*, 1983, pp. 30–36.

[15] K. Aihara, Y. Sakata, and N. Tago, "Ultra-high bandwidth heat resistance leaky coaxial cable," in *Int. Wire Cable Symp. Proc.*, 1992, pp. 732–738.

[16] I. Sakabe, K. Aihara, S. Hisano, Y. Sakata, and S. Suzuki, "Design of a VHF–UHF super-broadband leaky coaxial cable (LCX)," *Sumitomo Electr. Tech. Rev.*, no. 39, pp. 57–61, Jan. 1995.

[17] R. E. Collin and F. J. Zucker, *Antenna Theory.* New York: McGraw-Hill, 1969.

[18] M. Abramowitz and I. A. Stegun, *Handbook of Mathematical Functions.* Washington, D.C.: U.S. Dept. Commerce, 1982.

Seon-Taek Kim received the B.S. and M.S. degrees in electronic engineering from Yonsei University, Seoul, Korea, in 1992 and 1994, respectively, and is currently working toward the Ph.D. degree.

Since 1993, he has been at the Radio Communications Research Center, Yonsei University. From 1992 to 1993, he studied mobile antennas suited for underground, and his theoretical results have been successfully applied in the subway communication systems of Seoul, Korea. From 1994 to 1995, he joined in the development of RF converters for code division multiple access (CDMA) base stations. Since 1996, he has been engaged in the research of adaptive array antenna for mobile communications.

Gi-Ho Yun received the B.S. and M.S. degrees in electronic engineering from Yonsei University, Seoul, Korea in 1984 and 1986, respectively, and is currently working toward the Ph.D. degree.

From 1986 to 1992, he was engaged in the development of low-noise and high-power transceivers for satellite communications at the Samsung Advanced Institute of Technology. In 1993, he was with the Samsung Electro-Mechanics Corporation Research Center developing RF systems for cellular phones. His current research interests include a design of RF components using new materials, and monolithic microwave integrated circuits (MMIC's).

Han-Kyu Park (M'82–SM'82) received the B.S. and M.S. degrees in electrical engineering from Yonsei University, Seoul, Korea, in 1964 and 1968, respectively, and the Ph.D. degree in electronic engineering from Paris VI University, Paris, France in 1975.

Since 1976, he has been teaching in the Department of Electronic Engineering, Yonsei University. From 1979 to 1980, he was a Visiting Professor in the Department of Electrical Engineering, Stanford University. From 1985 to 1988, he served as a Member of the Technical Committee of the 1988 Seoul Olympics, and as a Member of the Advisory Committee for the 21st Century under direct control of the President from 1989 to 1994. Since 1991, he has joined the G-7 Planning Committee, Ministry of Trade and Industry. From 1995 to 1996, he was the President of the Korean Institute of Communication Sciences. Since 1993, he has served as the Head of the Radio Communications Research Center, Yonsei University. His interests include wireless mobile communications, radio technology, communication networks, and optical signal processing.

Dr. Park was the recipient of three scientific awards from the Korean Institute of Electrical Engineers (1976), the Korean Institute of Telematics and Electronics (1978), and the Korean Institute of Communication Sciences (1986), respectively.